D-1-3

Extended Abstracts of the 2011 International Conference on Solid State Devices and Materials, Nagoya, 2011, pp829-830

An Accurate Prediction Model of Temperature Dependent Current Mismatch in All Inversion and Influence of Subthreshold Hump on Mismatch Characteristics

Kiyohiko Sakakibara, Kazutami Arimoto

Renesas Electronics Corp., 4-1 Mizuhara, Itami, Hyogo 664-0005, Japan

Phone: +81-72-787-2709, Fax: +81-72-789-3009, E-mail: kiyohiko.sakakibara.wx@renesas.com

Abstract

We have found and verified that the standard deviation of current mismatch σ(ΔI/I) can be precisely expressed based on trans-conductance efficiency g_m/I when MOSFET doesn't have the subthreshold hump. Especially, it is verified for the first time that temperature dependence of σ(ΔI/I) in all inversion can be predicted within +/-10% accuracy with our model. As a result, influence of the subthreshold hump on MOSFET current mismatch is clarified.

1. Introduction

Importance of MOSFET current mismatch prediction increases with decrease in desired power-consumption level [1]. To design an analog circuit with small area and low power for portable or bio-signal sensing applications [2], precise σ(ΔI/I) prediction in weak inversion is indispensable. There are some models that try to predict σ(ΔI/I) curve [3][4]. However, they need to adjust the fitting parameters depending on channel size, and the accuracy in weak inversion is not in an allowable level. As a reason for the low prediction accuracy in weak inversion, an influence of the subthreshold hump is supposed [4][5]. In nanoscale MOSFET with STI, avoiding an influence of the subthreshold hump becomes more difficult [6].

A temperature dependence of current mismatch is also discussed in some papers [7][8], but a reproducibility of σ(ΔI/I) curve in all inversion is not available.

2. Influence of subthreshold hump on current mismatch

By displaying Vg-Id curves of some pair-transistors at the same time, a hump can be identified as shown in Fig. 1. A hump in the subthreshold region appears when channel has plural different barrier heights to carrier excitation from source to channel. To obtain the hump depicted in Fig. 1-1, STI formation condition is experimentally changed.

An existence of a hump can be detected in high sensitivity by evaluating σ(ΔI/g_m)=σ(ΔI/I)/(g_m/I) curve, as depicted in Fig. 2. When a hump exists, σ(ΔI/g_m) in weak inversion increases with decrease in channel current. The similar increasing behavior of σ(ΔI/g_m) in weak inversion were reported [3][9]. But, its mechanism has not been clarified. On the other hand, when a hump doesn't exist, σ(ΔI/g_m) decreases with decrease in channel current. From Fig. 2, it is clear that the increasing behavior of σ(ΔI/g_m) in weak inversion are caused by the subthreshold hump.

Also in channel size dependence of σ(ΔI/I) curve, an influence of a hump can be clearly seen as depicted in Fig. 3. When a hump exists, σ(ΔI/I)×√($L_{eff}W_{eff}$) in weak inversion depends on its channel size. On the other hand, when a hump doesn't exist, σ(ΔI/I)×√($L_{eff}W_{eff}$) of various channel sizes are merged into one curve. As shown in Fig. 3-2, the behavior of σ(ΔI/I)×√($L_{eff}W_{eff}$) curve is similar with that of g_m/I curve. The g_m/I universality is well known as the key parameter for analog circuit design [10].

3. Accurate prediction model of current mismatch

The similar behavior between σ(ΔI/I) and g_m/I is due that σ(ΔI/I) can be precisely expressed from g_m/I. Mathematical scheme is shown in Table I. In eq. (1), a reciprocal of g_m/I is expressed as a sum of reciprocals of each asymptote in weak and strong inversions. This is similar to Mattiessen's rule concerning the mobility. The maximum value 'c' in weak inversion equals q/nk_BT. By considering the difference of eq. (1) between adjacent MOSFET channels, eq. (2) can be obtained. We have confirmed that σ(ΔI/I) can be expressed as κ×σ(ΔI/I-Δg_m/g_m). In addition, κ is slightly lower than 1 and hardly depends on channel current. Thus, we assumed κ=1. Finally, as shown in eq. (4) and eq. (5), σ(ΔI/I)×√($L_{eff}W_{eff}$) can be obtained by η×g_m/I.

When a hump doesn't exist, we have found that η=σ(ΔI/g_m)×√($L_{eff}W_{eff}$) in weak inversion converges on a specific value of A_s which doesn't depend on channel size and temperature, as shown in Fig. 4. From eq. (5), A_s can be analytically expressed as σ(Δc/c)/c. Here c equals q/nk_BT. Namely, A_s is determined by the substrate factor 'n'. The value of 'n' depends on local channel characteristics [11]. This means that A_s is determined by channel factor.

An accuracy of our prediction model is verified. It is indicated in Fig. 5 that σ(ΔI/I)×√($L_{eff}W_{eff}$) curve at each temperature can be accurately predicted in all inversion by our model. It is shown in Fig. 6 that differences between the measured data and our model are within +/-10%. Parameters are extracted from each merged curve in Fig.3-2. We have confirmed that temperature dependent parameters are distributed in the straight line on the Arrhenius plot.

The specific value A_s can become another candidate for the current fluctuation indicator like Pelgrom and Takeuchi Vth-fluctuation indexes [12][13]. Unlike the Pelgrom index, a prediction of σ(ΔI/I) temperature dependence is also possible by using a constant A_s for a channel. It is shown in Fig. 5 that the measurement data can be predicted with an allowable accuracy by A_s×g_m/I(T,L,W). g_m/I(T,L,W) indicates g_m/I which is measured at each temperature and each channel size. This means that A_s becomes a current fluctuation indicator as long as the merged σ(ΔI/I)×√($L_{eff}W_{eff}$) curve depicted in Fig. 3-2 can be obtained in relatively wide channel transistors.

4. Conclusion

It has been revealed that σ(ΔI/I) behavior can be precisely derived and verified based on the g_m/I universality, as long as MOSFET doesn't have the subthrehold hump. An influence of the subthreshold hump should be avoided in order to predict MOSFET current mismatch accurately. For the first time, we have succeeded in a prediction of σ(ΔI/I) temperature dependence in all inversion with our model. This model is very profitable to an area reduction design of a low-power consumption analog circuit.

References

[1] E. Vittoz, ASSCC, p.129, 2009. [2] D. Yeager *et* al., *J.S.S.C.*, vol. 45, p.2198, 2010. [3] J. A. Croon *et* al., *J.S.S.C.*, vol. 37, p.1056, 2002. [4] C. Galup-Montoro *et* al., *J.S.SC.*, vol. 40, p.1649, 2005. [5] J. Pineda-Gyvez *et* al., J.S.S.C., vol. 39, p157, 2004. [6] A. Mizumura *et* al., ICMTS, p.39, 2005. [7] L. Vancaillie *et* al., ESSCIRC, p. 671, 2003. [8] P. Andricciola *et* al., EDL, vol. 30, p. 690, 2009. [9] Y. Joly *et* al., ICSICT, p.1817, 2010. [10] D. M. Binkley, Tradeoffs and Optimization in Analog CMOS Design, Willy, 2008. [11] Y. Tsividis, Operation and Modeling of the MOS Transistor, McGraw-Hill, 1999. [12] M.J.M.Pelgrom *et* al., *IEDM*, p.915, 1998. [13] K.Takeuchi *et* al., *IEDM*, p.467, 2007.

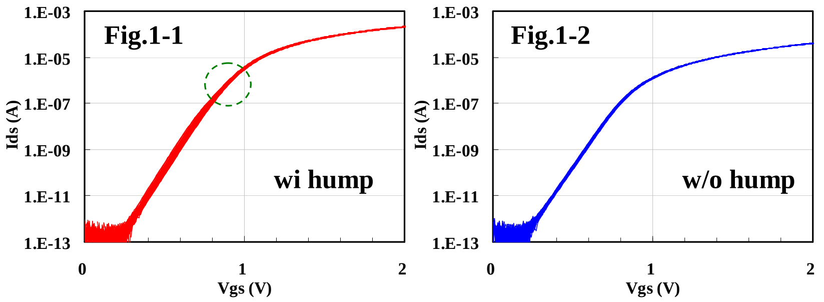

Fig.1 Measurement results of NMOS Vg-Id curves of 32 pair-transistors according to a presence of the subthreshold hump. In Fig.1-1, an existence of the subthreshold hump can be identified in the region enclosed with the circle. Also in Fig.1-1, it is hard to recognize a hump only in an individual curve. On the other hand, in Fig. 1-2, the subthreshold hump cannot be identified.

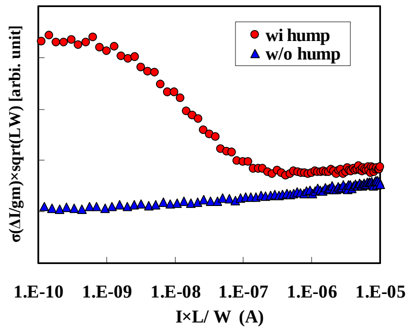

Fig.2 Measurement results of $\sigma(\Delta I/gm)$. Each curve of circle and triangle symbols is calculated from Vg-Id data of each pair shown in Fig.1. When a hump exists, $\sigma(\Delta I/gm)$ in weak inversion increases with decrease in channel current.

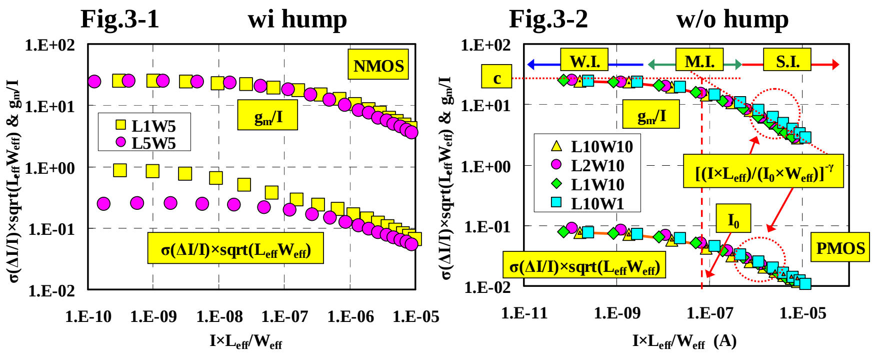

Fig.3 Channel size dependence of g_m/I and $\sigma(\Delta I/I)\times\sqrt{(L_{eff}W_{eff})}$ according to a presence of the subthreshold hump. As shown in Fig. 3-2, the merged curve of g_m/I has an asymptote of $(g_m/I)_{W.I.}=c$ (const.) in weak inversion, and has an asymptote of $(g_m/I)_{S.I.}=[(I\times L_{eff})/(I_0\times W_{eff})]^{-\gamma}$ in strong inversion, respectively. When MOSFET doesn't have a hump, behavior of $\sigma(\Delta I/I)\times\sqrt{(L_{eff}W_{eff})}$ curve is similar to that of the universal g_m/I curve. Gate oxide thickness measured in each figure is different.

Table I Mathematical scheme.

$$\frac{1}{\left(\frac{g_m}{I}\right)} = \frac{1}{\left(\frac{g_m}{I}\right)_{W.I.}} + \frac{1}{\left(\frac{g_m}{I}\right)_{S.I.}} = \frac{1}{c} + \frac{1}{\left(\frac{I}{I_0}\cdot\frac{L}{W}\right)^{-\gamma}} \quad \text{Eq. (1)}$$

, where $I_0=2n\mu C_{ox}(k_BT/q)^2$. (moderate inversion center)

$$\Delta left = \frac{\left(\frac{\Delta I}{I}-\frac{\Delta g_m}{g_m}\right)}{\left(\frac{g_m}{I}\right)} = \left[\frac{1}{c}\left(-\frac{\Delta c}{c}\right)+\frac{1}{\left(\frac{I}{I_0}\cdot\frac{L}{W}\right)^{-\gamma}}\left(\frac{\Delta\alpha}{\alpha}\right)\right] = \Delta right \quad \text{Eq. (2)}$$

$$\left(\frac{\Delta\alpha}{\alpha}\right) = -\gamma\frac{\Delta I_0}{I_0}+\gamma\frac{\Delta L}{L}-\gamma\frac{\Delta W}{W} \quad \text{Eq. (3)}$$

$$\sigma\left(\frac{\Delta I}{I}\right) = \frac{1}{\sqrt{L_{eff}W_{eff}}}\frac{g_m}{I}\cdot\eta \quad \text{Eq. (4)}$$

$$\eta = \sqrt{\left[\left\{\frac{1}{c}\sigma\left(\frac{\Delta c}{c}\right)\right\}^2+\left\{\frac{1}{\left(\frac{I}{I_0}\cdot\frac{L}{W}\right)^{-\gamma}}\sigma\left(\frac{\Delta\alpha}{\alpha}\right)\right\}^2\right]} \quad \text{Eq. (5)}$$

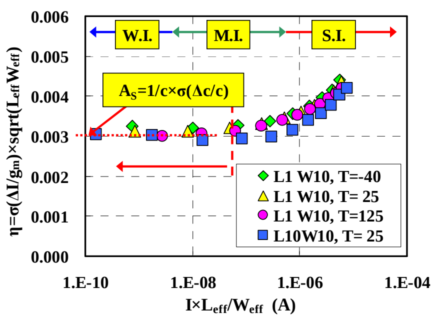

Fig.4 Measurement results of $\sigma(\Delta I/g_m)$. $\sigma(\Delta I/g_m)$ curves are obtained by using g_m/I and $\sigma(\Delta I/I)$ which are depicted in Fig. 3-2. In addition, temperature dependence is also depicted.

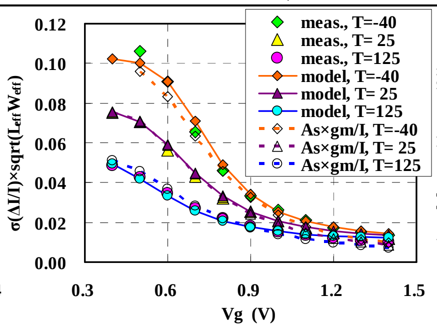

Fig.5 Comparison of $\sigma(\Delta I/I)\times\sqrt{(L_{eff}W_{eff})}$ between the measurements and two prediction methods. One is the model calculation shown in Table I. (solid lines) Another is calculated by $A_s\times g_m/I(T,L,W)$.(dotted lines)

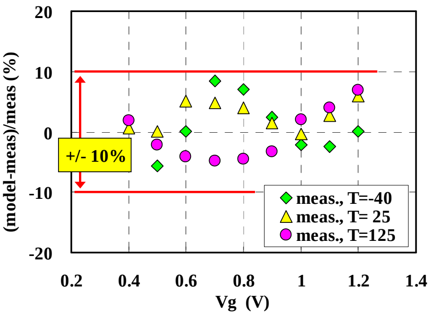

Fig.6 Relative difference between the measurements and the model calculations at -40, 25, and 125 deg-C.